efficiency or because of direct inhibitory effects of high thoracic temperatures on the flight musculature. Force production by tethered honeybees decreases by 45% as thoracic temperature rises from 39° to 45°C (*16*), similar to the decrease in metabolic rate we observed over the same thoracic temperature range (Figs. 2 and 3A).

Variation in heat production may explain thermal stability during flight in other endothermic insects and potentially could contribute to thermoregulation in birds (*17*). Although heat production does not vary with air temperature in moths or bumblebees, which can shunt heat to the abdomen to increase heat loss (*1*), many endothermic insects lack the capacity to modulate heat transfer between thorax and abdomen (*1, 2*). Wing-beat frequencies and flight metabolic rates have also been reported to decrease with air temperature in bees of the genus *Centris* (*18, 19*). Wing-beat frequencies and inferred heat production decline at higher air temperatures in the dragonfly *Anax junius* (*20*), suggesting that the role of varying heat production in achieving thermal stability during flight may deserve a general reevaluation for large endothermic insects. For insects in which flight metabolic rate varies with air temperature, it will be important to reexamine energetic models of migration, foraging, and mating for temperature sensitivity.

REFERENCES AND NOTES

1. B. Heinrich, *The Hot-Blooded Insects* (Harvard Univ. Press, Cambridge, 1992); _____ and H. Esch, *Am. Sci.* **82**, 164 (1994).
2. T. M. Casey, *Adv. Insect Physiol.* **20**, 120 (1988).
3. B. Heinrich, *J. Exp. Biol.* **80**, 217 (1979).
4. _____, *ibid.* **85**, 73 (1980).
5. _____, *ibid.*, p. 61; P. D. Cooper, W. M. Schaffer, S. L. Buchmann, *ibid.* **114**, 1 (1985).
6. T. M. Casey, in *Insect Flight*, G. J. Goldsworthy and C. H. Wheeler, Eds. (CRC Press, Boca Raton, FL, 1989), pp. 257–272.
7. J. F. Harrison and H. G. Hall, *Nature* **363**, 258 (1993).
8. Metabolic rates were calculated during 1 min of flight from carbon dioxide emission by flow-through respirometry, with flow rates of 2 liter min^{-1} (measured with an Omega mass flow meter), a 300-ml lucite respirometry chamber, and a LICOR 5152 CO_2 analyzer, assuming a respiratory quotient of 1.0 (*7*). Wing-beat frequencies were measured with digitized tape recordings and SoundEdit (*7*). In all instances, bees were tested within 5 min of capture.
9. After completion of the metabolism measurements, bees were shaken out of the respirometry chamber into a plastic bag and restrained against a plastic foam surface. Thoracic and abdominal temperatures were measured within 10 s of flight by inserting a Physitemp model MT-29/1 hypodermic microprobe (time constant, 0.025 s) into first the thorax and then the abdomen.
10. J. F. Harrison, D. I. Nielsen, R. E. Page, *Funct. Ecol.* **10**, 81 (1996).
11. Loaded bees were collected after feeding ad libitum from a 1 M sucrose solution. Unloaded bees were collected as they arrived at the feeder. Metabolic rates during agitated flight were measured as described (*7, 8*).
12. Metabolic rates of hovering European honeybees from a single colony at Arizona State University, Tempe, were measured in a vertical Plexiglas cylinder (internal diameter, 51 mm) by measuring carbon dioxide emission by flow-through respirometry essentially as described (*7, 8*), except that flow rates through the chamber averaged 2 to 4 liter min^{-1}. Data are reported only for the small fraction of bees that hovered without any provocation, in the center of the tube, with less than 1 cm of verticle movement during the respirometry measurements.
13. M. H. Dickinson and J. R. B. Lighton, *Science* **268**, 87 (1995).
14. C. P. Ellington, *Philos. Trans. R. Soc. London Ser. B* **305**, 1 (1984).
15. H. G. Spangler and S. L. Buchmann, *J. Kans. Entomol. Soc.* **64**, 107 (1991).
16. J. R. Coelho, *Physiol. Zool.* **64**, 823 (1991).
17. K. L. Schuchman, *Ibis* **121**, 85 (1979).
18. H. G. Spangler, *Bee Sci.* **2**, 181 (1992).
19. S. P. Roberts, N. F. Hadley, J. F. Harrison, *Am. Zool.* **34**, 142 (1994).
20. M. L. May. *J. Exp. Biol.* **198**, 2385 (1995).

21. We thank R. Page and D. Nielsen for providing bees and for help at the University of California, Davis. We thank the members of the Escuela Agricola Panamericana, Zamorano, Honduras, for help with the African bee portion of this project. R. Dudley and three anonymous reviewers made helpful comments on a version of this manuscript. Supported by grants from the NSF and a Faculty Grant-in-Aid award from Arizona State University to J.F.H., a First Award from the National Institutes of Health to J.H.F., and a USDA National Research Initiative Competitive Grant and US-AID Program Support Grant to H.G.H.

10 May 1996; accepted 16 August 1996

A Cellular Homolog of Hepatitis Delta Antigen: Implications for Viral Replication and Evolution

Robert Brazas and Don Ganem*

Hepatitis delta virus (HDV) is a pathogenic human virus whose RNA genome and replication cycle resemble those of plant viroids. However, viroid genomes contain no open reading frames, whereas HDV RNA encodes a single protein, hepatitis delta antigen (HDAg), which is required for viral replication. A cellular gene whose product interacts with HDAg has now been identified, and this interaction was found to affect viral genomic replication in intact cells. DNA sequence analysis revealed that this protein, termed delta-interacting protein A (DIPA), is a cellular homolog of HDAg. These observations demonstrate that a host gene product can modulate HDV replication and suggest that HDV may have evolved from a primitive viroidlike RNA through capture of a cellular transcript.

HDV was originally discovered as a cause of severe liver injury in individuals already infected with hepatitis B virus (HBV) (*1*). The clinical association between these two viruses results from the fact that HDV does not encode an envelope protein; instead, its genome is enveloped by HBV surface glycoproteins during virus assembly (*2*). The HDV genome comprises a 1700-nucleotide (nt) single-stranded circular RNA that is ~70% self-complementary and, as a result, forms a highly base-paired rodlike structure (*3*). This genome encodes only one known viral protein, HDAg, a nuclear phosphoprotein (*4*) capable of specific binding to HDV RNA (*5*). HDAg is absolutely required for HDV genomic replication (*6*), but the mechanism by which it influences RNA synthesis is unknown.

The HDV genome strongly resembles those of viroids, small naked infectious RNA molecules that produce epidemic disease in many varieties of plants (*7*). Like HDV, viroid genomes are covalently closed, single-stranded circular RNAs with extensive self-complementarity. As in HDV, these viroid RNAs form highly base-paired RNA rods. Viroid RNAs possess ribozyme activities that catalyze RNA self-cleavage and self-ligation (*8*), and similar catalytic activities have been detected in HDV RNA (*9*). However, viroid RNAs are much smaller (<400 nt) and have no open reading frames.

In the currently accepted model of HDV replication, which is based on schemes originally proposed for viroids (*10*), the incoming HDV genome serves as a template for rolling circle replication, resulting in the production of complementary multimeric antigenomes. Nascent antigenomes use their intrinsic ribozyme activities to catalyze self-cleavage and self-ligation, producing circular monomeric antigenomic RNAs. Through a similar rolling circle mechanism, these antigenomes then serve as templates for the production of additional HDV genomic RNAs. Although HDAg is required for replication, it has no known polymerase activity, implying that a host polymerase mediates replication. On the basis of the sensitivity of HDV RNA replication to α-amanitin, the responsible host enzyme has been suggested to be RNA polymerase II (*11*).

Because HDV replication requires HDAg, we speculated that this viral protein might interact with one or more cellular proteins (for example, basal or accessory transcription factors) to promote HDV replication. Accordingly, we used the yeast two-hybrid assay to

R. Brazas, Departments of Microbiology and Medicine, University of California, San Francisco, CA 94143, USA. D. Ganem, Howard Hughes Medical Institute and Departments of Microbiology and Medicine, University of California, San Francisco, CA 94143, USA.

*To whom correspondence should be addressed.

search for cellular factors that interact with HDAg. Yeast expressing a fusion protein comprising the DNA binding domain of Gal4p and HDAg were transformed with a library of human cDNAs that were fused to the sequence encoding the Gal4p activation domain (*12*). Of ~2×10^6 independent transformants, 19 were selected on the basis of their ability to activate transcription of a *HIS3* reporter gene under the control of multiple Gal4p binding sites. From these 19 original His^+ transformants, 12, each of which contained a fragment (800 to 900 nt) of the same cDNA sequence, were reproducibly positive. We refer to the protein product of this cDNA as DIPA (delta-interacting protein A), and to the corresponding gene as *DIPA*. The size of the *DIPA* mRNA (1.1 kb) indicated that the *DIPA* cDNA clones isolated in the two-hybrid analysis were likely missing 100 to 200 nt at their 5′ termini (*13*). With a polymerase chain reaction (PCR)–based approach (*14*), we were able to clone a cDNA corresponding to the 5′ end of the transcript. A complete *DIPA* cDNA was then reconstructed by combining this 5′ PCR product with the previously identified *DIPA* cDNAs.

Northern blot analysis with a *DIPA*-specific probe revealed that *DIPA* mRNA is present in the human hepatic cell line HepG2 and in most human tissues, including liver (Fig. 1). DIPA protein was also detected in uninfected HepG2 cells by immunoblot analysis of immunoprecipitates prepared with antibodies to DIPA (*15*). Although HDV RNA in infected humans is present predominantly in liver (*1*, *2*), this is likely the result of the restricted tissue tropism of its HBV helper. Transient transfection of cultured cells with HDV sequences has shown that nonhepatic cell types are permissive for HDV RNA replication (*6*), and widespread replication of HDV is apparent in transgenic mice bearing viral DNA (*16*).

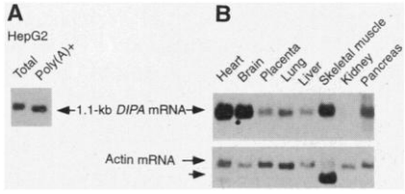

Fig. 1. Northern blot analysis of *DIPA* expression. (**A**) Expression of *DIPA* in HepG2 cells. Total RNA (10 μg) and poly(A)$^+$ RNA (0.5 μg) were analyzed by nonradioactive Northern blot analysis with a *DIPA*-specific riboprobe uniformly labeled with digoxigenin, which was subsequently detected with alkaline phosphatase–conjugated antibodies to digoxigenin (*13*). (**B**) Expression of *DIPA* in human tissues. A multiple-tissue Northern blot was also hybridized with the *DIPA*-specific riboprobe (top row) and, subsequently, with an actin-specific riboprobe (bottom row). The positions of the 1.1-kb *DIPA* mRNA and of actin mRNAs are indicated.

Nucleotide sequence analysis of the *DIPA* cDNA revealed that the gene encodes a polypeptide whose predicted primary sequence is 24% identical to that of HDAg (Fig. 2). If conservative substitutions are also taken into account, the sequence similarity between the two proteins increases to 56%. At 202 amino acids, DIPA is similar in size to HDAg, and the DIPA-HDAg homology extends over the entire length of both proteins, including the distinctive proline- and glycine-rich region of the HDAg COOH-terminus. In fact, the similarity extends beyond the UAG stop codon of the classical 24-kD HDAg. During HDV replication, some HDV RNAs undergo specific editing at this UAG codon that converts it to UGG and allows translation to continue to the next in-frame stop codon (*2*). This process results in the production of the so-called large HDAg, which contains an additional 19 amino acids at the COOH-terminus. The homology between DIPA and HDAg includes this COOH-terminal extension. DIPA contains two leucine heptad repeats with the potential to form coiled-coil protein-interaction domains. HDAg also contains such a domain (*17*, *18*), which is responsible for the homomultimerization of the protein. The central region of HDAg contains two arginine-rich motifs (ARMs) that are implicated in RNA binding (*19*); DIPA has retained at least one such motif, although it is not yet clear whether it serves a similar function.

In addition to its homology to HDAg, the amino acid sequence of DIPA also shows similarity to the transcription factor FRA1 and other FRA family members. The homology is limited to the FRA bZIP (basic region–leucine zipper) DNA binding and dimerization domain (amino acids 43 to 180 of rat FRA1), which is 35% identical to amino acids 19 to 147 of DIPA (*20*). Thus, the DIPA sequence is consistent with it being a nucleic acid–binding protein, possibly even a transcription factor, although the role of the protein in uninfected cells remains to be determined.

To verify that DIPA and HDAg interact in intact mammalian cells, we performed coimmunoprecipitation experiments. Human embryonic kidney 293T cells were transfected either singly or doubly with plasmid-based expression vectors for HDAg and DIPA, the latter bearing an epitope tag from influenza hemagglutinin (the encoded protein was designated HA-DIPA). Immunoblot analysis of extracts of transfected cells with antibodies to either HDAg or DIPA (prepared against recombinant DIPA protein) revealed that each protein was expressed in cells transfected with the appropriate vector (Fig. 3, A and B, lanes 2, 3, and 6). Each lysate was then subjected to immunoprecipitation with monoclonal anti-

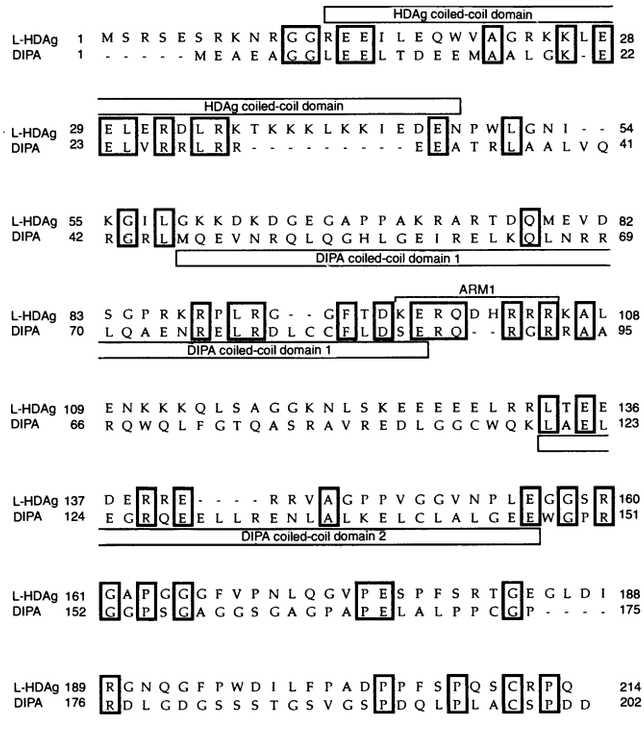

Fig. 2. Comparison of amino acid sequences of large HDAg (L-HDAg) and DIPA. Sequence alignment was performed with the GAP program (Wisconsin Genetics Computer Group) with a gap creation penalty of 3.0 and a gap extension penalty of 0.1. After alignment with GAP, the similarity was determined with the Seq-Vu program and the GES scales (*23*), with a similarity cutoff of ≥85% required for the similarity to be noted. Identical residues are boxed, and similar residues are identified by shading. The predicted coiled-coil regions of DIPA were identified with the COILS2 program (*24*) and are indicated with labeled boxes. The start of each predicted coiled-coil domain of DIPA corresponds to the "a" position of the predicted heptad repeats "a" through "g." The coiled-coil domain and the first arginine-rich RNA binding motif (ARM1) of HDAg are also indicated. Residue numbers are shown at the ends of each line for both sequences.

bodies to HA (*21*), and the immunoprecipitates were examined by immunoblot analysis with antibodies to DIPA or to HDAg (Fig. 3, C and D). As expected, HA-DIPA was detected in all precipitates prepared from HA-DIPA–expressing cells (Fig. 3C, lanes 3 and 6). In contrast, HDAg was detected only in the anti-HA immunoprecipitates prepared from cells co-expressing HDAg and HA-DIPA (Fig. 3D, lanes 2 and 6). Thus, the interaction between HDAg and DIPA occurs in mammalian cells as well as in yeast, and was not due to the use of artificial Gal4p fusion constructs.

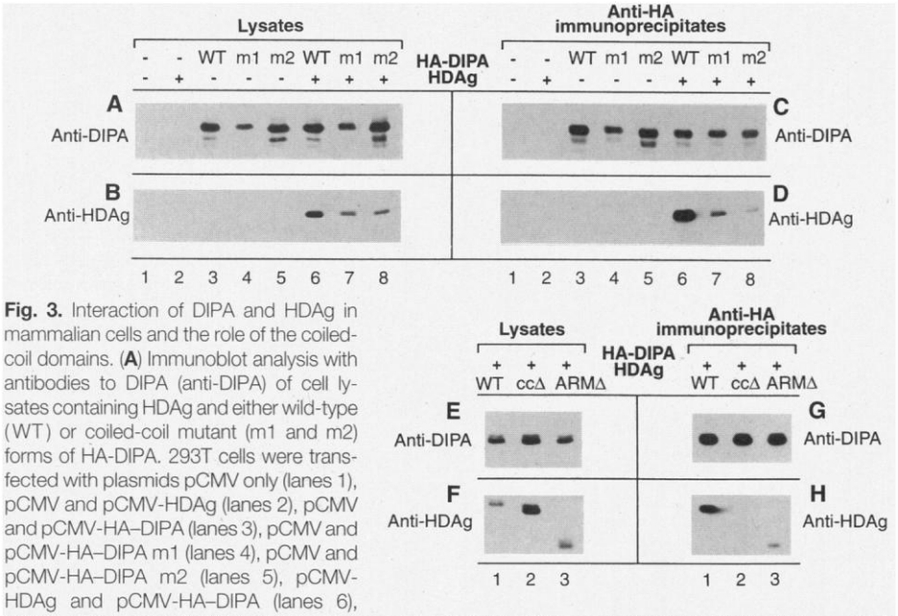

Fig. 3. Interaction of DIPA and HDAg in mammalian cells and the role of the coiled-coil domains. (**A**) Immunoblot analysis with antibodies to DIPA (anti-DIPA) of cell lysates containing HDAg and either wild-type (WT) or coiled-coil mutant (m1 and m2) forms of HA-DIPA. 293T cells were transfected with plasmids pCMV only (lanes 1), pCMV and pCMV-HDAg (lanes 2), pCMV and pCMV-HA–DIPA (lanes 3), pCMV and pCMV-HA–DIPA m1 (lanes 4), pCMV and pCMV-HA–DIPA m2 (lanes 5), pCMV-HDAg and pCMV-HA–DIPA (lanes 6), pCMV-HDAg and pCMV-HA–DIPA m1 (lanes 7), or pCMV-HDAg and pCMV-HA–DIPA m2 (lanes 8). A portion (1%) of soluble lysate of transfected cells was fractionated by SDS–polyacrylamide gel electrophoresis (12.5% gel), transferred to a membrane, and subjected to immunoblot analysis with anti-DIPA. (**B**) Immunoblot analysis as in (A) with anti-HDAg. The reduced amount of HDAg in lane 2 compared with lane 6 suggests that HDAg is stabilized by co-expression of DIPA. (**C**) Immunoblot analysis with anti-DIPA of anti-HA immunoprecipitates. Lysates from (A) and (B) were subjected to immunoprecipitation with HA-specific antibodies, and one-third of the resulting precipitates was subjected to immunoblot analysis with anti-DIPA. (**D**) Immunoblot analysis with anti-HDAg of anti-HA immunoprecipitates. The remaining two-thirds of the anti-HA immunoprecipitates from (C) were subjected to immunoblot analysis with anti-HDAg. (**E** through **H**) The role of coiled-coil domains in the interaction of DIPA and HDAg. 293T cells were transfected with plasmids pCMV-HA–DIPA and pCMV-HDAg (lanes 1), pCMV-HA–DIPA and pCMV-HDAg ccΔ (deletion of amino acids 19 to 31 of HDAg coiled-coil domain) (lanes 2), or pCMV-HA–DIPA and pCMV-HDAg ARMΔ (deletion of amino acids 89 to 145 of HDAg containing the two ARMs) (lanes 3). Lysates (E and F) and anti-HA immunoprecipitates (G and H) were prepared and subjected to immunoblot analysis with anti-DIPA (E and G) or anti-HDAg (F and H) as described for (A) through (D).

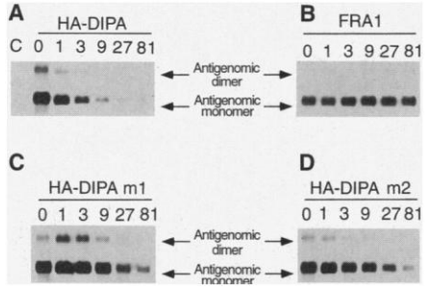

Fig. 4. Effect of overexpression of DIPA on HDV replication. (**A**) 293T cells were transfected with 3 μg of pSVL-D3 (HDV genomic trimer RNA expression vector) and threefold increasing amounts of pCMV-HA–DIPA expression vector shown above each lane, where 1 corresponds to 0.11 μg of the HA-DIPA expression plasmid. As a negative control, cells in lane C were transfected with 3 μg of pSVL (the parent vector of pSVL-D3 lacking HDV sequences). Two days after transfection, the cells were plated in medium containing hygromycin (200 μg/ml). (The pCMV vectors encode resistance to hygromycin.) The medium was changed approximately every 3 days. Nine days after transfection, total RNA was isolated from the transfected cells, and 3 μg from each sample were subjected to nonradioactive Northern blot analysis with an HDV antigenome–specific riboprobe uniformly labeled with digoxigenin. (**B**) Effect of overexpression of FRA1, a protein with sequence similarity to DIPA (*20*), on HDV replication. The same experiment as in (A) was performed with the exception that pCMV-FRA1 was substituted for pCMV-HA–DIPA. (**C** and **D**) Effects of HA-DIPA coiled-coil mutants m1 and m2 on HDV replication. The same experiment as in (A) was performed with the exception that pCMV-HA–DIPA m1 (C) or pCMV-HA–DIPA m2 (D) was substituted for pCMV-HA–DIPA. The positions of antigenomic dimers and monomers are indicated.

To determine the roles of the coiled-coil domains of DIPA and HDAg in this interaction, we tested the effects of mutations in these regions on HDAg-DIPA coprecipitation. DIPA mutant m1 contains a two–amino acid insertion at residue 67 of coiled-coil domain 1, and mutant m2 contains a similar insertion at residue 127 of coiled-coil domain 2. Each mutation markedly impaired the binding of DIPA to HDAg, with the m2 insertion showing the greatest effect (Fig. 3, C and D, lanes 6 to 8). We performed a similar analysis for an HDAg mutant (ccΔ) with a 13–amino acid deletion within the coiled-coil region (*17*, *18*) (Fig. 3, E through H). This mutation completely prevented DIPA binding by HDAg (Fig. 3, G and H, lanes 1 and 2). In contrast, deletion of 57 amino acids from the central region of HDAg (ARMΔ mutant) did not eliminate DIPA binding (Fig. 3, G and H, lane 3). These data indicate that the interaction between DIPA and HDAg requires coiled-coil motifs of each partner. The larger effect of the HDAg ccΔ mutation is likely due to the greater disruption of the coiled-coil structure caused by this deletion.

To determine whether the DIPA-HDAg interaction has consequences for viral replication, we examined the effects of DIPA overexpression on HDV genomic RNA synthesis. 293T cells were transfected with a fixed quantity of the plasmid pSVL-D3, which encodes HDV genomic multimers capable of replication, and increasing amounts of either the wild-type HA-DIPA expression vector (pCMV-HA–DIPA) or a control FRA1 expression vector (pCMV-FRA1). After 9 days, total RNA was extracted and examined by Northern blot analysis for the presence of monomeric antigenomic HDV RNA, which can be produced only by authentic HDV replication. Overexpression of wild-type DIPA markedly inhibited HDV replication, whereas similar overexpression of FRA1 had no effect on HDV RNA synthesis (Fig. 4, A and B). The observed inhibition was not due to nonspecific toxicity of DIPA, because the expression of a cotransfected human growth hormone reporter construct in these cells was not impaired (*15*). DIPA is a potent inhibitor of HDV replication; inhibition was apparent when as little as 0.1 μg of pCMV-HA–DIPA was cotransfected with 3 μg of pSVL-D3 (Fig. 4A, lane 1). When DIPA mutants m1 and m2 were similarly assayed (Fig. 4, C and D), the inhibition of HDV replication was markedly attenuated; inhibition of replication was observed at high concentrations of the mutant constructs (Fig. 4, C and D, lanes 27 and 81), consistent with the observation that these mutations do not completely abolish the in-

teraction with HDAg (Fig. 3). These results show that DIPA overexpression can specifically down-regulate HDV RNA synthesis, and they raise the possibility that DIPA may be a negative regulator of HDV replication in vivo, in which case one function of HDAg in replication could be to relieve this inhibition by forming a complex with DIPA. Consistent with this model, HDAg overexpression reversed the inhibition of HDV replication observed in cells overexpressing a fixed amount of DIPA (Fig. 5). The mechanism by which DIPA might exert this negative regulation is not known; its elucidation will require a better understanding of the normal function of DIPA in uninfected cells.

The relation between HDAg and DIPA also has implications for the evolution of HDV. Branch *et al.* (*22*) noted that the structural and catalytic elements of HDV RNA that resemble those of viroids are clustered in one region of the RNA, separate from the HDAg coding region, and therefore speculated that HDV might have evolved from a viroidlike RNA by capture of a cellular transcript. Our identification of DIPA and its homology to HDAg support this idea. We propose that in nuclei infected with a primitive viroidlike RNA, a template transfer occurred from a replicative intermediate to the 3′ end of the evolutionary ancestor of *DIPA* mRNA. Because the most abundant growing RNA strands in infected cells are of genomic polarity, the most likely strand to be transferred would be of this polarity. Transfer of this nascent genomic strand to a *DIPA*-like mRNA or precursor mRNA, followed by copying of this template, would result in the capture of *DIPA* sequences. We propose that, after copying to the 5′ end of the *DIPA* template, a hairpin formed at the 3′ end of the newly synthesized RNA would allow synthesis to continue to complete the newly formed HDV genome. Further evolution would allow the opposite halves of the genome to diverge to the level of 70% complementarity that now exists. The final structure of the fusion RNA would have genomic viroid sequences linked to the complement of the *DIPA* coding sequences: exactly the polarity of modern-day HDV.

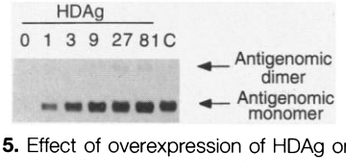

Fig. 5. Effect of overexpression of HDAg on the inhibition of HDV replication by DIPA overexpression. 293T cells were transfected with 3 μg of pSVL-D3 (HDV genomic trimer RNA expression vector), 3 μg of pCMV-HA–DIPA, and threefold increasing amounts of pCMV-HDAg expression vector shown above each lane, where 1 corresponds to 0.11 μg of the HDAg expression plasmid. As a positive control for HDV replication, cells in lane C were transfected with 3 μg of pSVL-D3 and 13 μg of pCMV vector only. Two days after transfection, the cells were plated into medium containing hygromycin (200 μg/ml). The medium was changed approximately every 3 days. Nine days after transfection, total RNA was isolated from the transfected cells, and 3 μg from each sample were subjected to nonradioactive Northern blot analysis with an HDV antigenome–specific riboprobe uniformly labeled with digoxigenin.

REFERENCES AND NOTES

1. M. Rizzetto, *Hepatology* **3**, 729 (1983).
2. A. Smedile, M. Rizetto, J. Gerin, *Prog. Liver Dis.* **12**, 157 (1994); M. Rizzetto *et al.*, *Proc. Natl. Acad. Sci. U.S.A.* **77**, 6124 (1980).
3. K. S. Wang *et al.*, *Nature* **323**, 508 (1986); A. Kos, R. Kijkema, A. Arnberg, P. van der Meide, H. Schellekens, *ibid.*, p. 558; P. J. Chen *et al.*, *Proc. Natl. Acad. Sci. U.S.A.* **83**, 8774 (1986); S. Makino *et al.*, *Nature* **329**, 343 (1987).
4. Y. P. Xia, C.-T. Yeh, J.-H. Ou, M. Lai, *J. Virol.* **66**, 914 (1992); M.-F. Chang, S. Chang, C.-I. Chang, K. Wu, H.-Y. Kang, *ibid.*, p. 6019; S. Hwang, C. Lee, M. Lai, *Virology* **190**, 413 (1992).
5. J.-H. Lin, M.-F. Chang, S. Baker, S. Govindarajan, M. Lai, *J. Virol.* **64**, 4051 (1990); M. Chao, S.-Y. Hsieh, J. Taylor, *ibid.* **65**, 4057 (1991).
6. M. Kuo, M. Chao, J. Taylor, *ibid.* **63**, 1945 (1989); J. Glenn, J. Taylor, J. White, *ibid.* **64**, 3104 (1990).
7. R. Symons, *Semin. Virol.* **1**, 75 (1990).
8. G. A. Prody, J. T. Bakos, J. M. Buzayan, I. R. Schneider, G. Breuning, *Science* **231**, 1577 (1986); A. Forster and R. Symons, *Cell* **50**, 9 (1987).
9. H.-N. Wu and M. M. C. Lai, *Science* **243**, 652 (1989); L. Sharmeen, M. Kuo, G. Dinter-Gottlieb, J. Taylor, *J. Virol.* **62**, 2674 (1988); H.-N. Wu and M. Lai, *Mol. Cell. Biol.* **10**, 5575 (1990); M. Kuo, L. Sharmeen, G. Dinter-Gottlieb, J. Taylor, *J. Virol.* **62**, 4439 (1988); L. Sharmeen, M. Kuo, J. Taylor, *ibid.* **63**, 1428 (1989).
10. A. D. Branch and H. D. Robertson, *Science* **223**, 450 (1984).
11. T. MacNaughton, E. Gowans, S. McNamara, C. Burrell, *Virology* **184**, 387 (1991); T.-B. Fu and J. Taylor, *J. Virol.* **67**, 6965 (1993).
12. The complete HDAg open reading frame (small HDAg) was cloned into the Gal4p DNA-binding domain vector pAS2 [J. W. Harper, G. Adami, N. Wei, K. Keyomarsi, S. J. Elledge, *Cell* **75**, 805 (1993)] and used as bait to screen the pGADNOT-HL-60 cDNA activation domain library [J. Luban, K. L. Bossolt, E. K. Franke, G. V. Kaplana, S. Goff, *ibid.* **73**, 1067 (1993)] for HDAg-interacting proteins as described by Harper *et al.* Nineteen original His$^+$ colonies were isolated, and, after rescreening and checking for specificity, 12 isolates were identified as true positives. The 12 clones were subjected to restriction mapping and shown to contain three classes of inserts. DNA sequencing revealed that the three classes (*DIPA-2*, *-17*, and *-7*) contained cDNAs that were derived from the same mRNA and differed only in their 5′ and 3′ ends.
13. Total RNA was isolated from HepG2 cells with RNAzol B (TEL-TEST), and polyadenylated [poly(A)$^+$] RNA was then purified from total RNA with Oligotex-dT (Qiagen). RNA samples were fractionated in a standard 1% agarose-formaldehyde gel, transferred to a positively charged nylon membrane (Boehringer Mannheim) under mild alkaline conditions, and fixed to the membrane as described [R. Low and T. Rausch, *Biotechniques* **17**, 1026 (1994)]. The human multiple-tissue Northern (RNA) blot was obtained from Clontech. The digoxigenin-labeled *DIPA*-specific (*DIPA* nucleotides 443 to 212) and actin-specific [from pTRI-β-actin template (Ambion)] riboprobes were synthesized with the use of a MEGAscript kit (Ambion) in combination with the digoxigenin RNA labeling mix (Boehringer Mannheim). The blots were prehybridized and hybridized essentially as described by Low and Rausch. After hybridization, the blots were washed (15 min per wash) at 72°C with solutions comprising 0.1% SDS and 2×, 0.5×, and 0.1× standard saline citrate, respectively, and the hybridized digoxigenin-labeled probes were detected essentially as described [G. Engle-Blum *et al.*, *Anal. Biochem.* **210**, 235 (1993)]. Exposures times varied between 1 and 60 min depending on the experiment.
14. The ligation-anchored PCR technique used to amplify and clone the 5′ end of the *DIPA* mRNA was performed basically as described [A. N. Apte and P. D. Siebert, *Biotechniques* **15**, 890 (1993)] with 1.5 μg of poly(A)$^+$ RNA isolated from 293T cells with the use of Oligotex-dT. The *DIPA* 5′-end cDNA product generated was T-A cloned into pBluescript II KS+ (Stratagene) as described [F. M. Ausubel *et al.*, Eds., *Current Protocols in Molecular Biology* (Wiley, Brooklyn, NY, 1994), vol. 2]. Three different clones were sequenced, and all three contained the same cDNA insert, which corresponded to a perfect extension of the 5′ end of the *DIPA-2* clone by an additional 150 base pairs (bp). This 5′ cDNA product was combined with the *DIPA-2* cDNA isolate with the use of a common Not I restriction site, generating the full-length *DIPA* cDNA clone. The complete *DIPA* cDNA was resequenced with the use of deoxyinosine triphosphate in the presence of 10% (v/v) dimethylsulfoxide as described [P. Winship, *Nucleic Acids Res.* **17**, 1266 (1989); D. DeShazer, G. E. Wood, R. L. Friedman, *Biotechniques* **17**, 288 (1994)]. The full-length *DIPA* cDNA comprised 879 bp, excluding the poly(A) tail. The AUG start codon of the open reading frame begins at nucleotide 29, and the last base of the UGA stop codon is at nucleotide 637. The sequence of the *DIPA* cDNA has been deposited in GenBank with the accession number U63825.
15. R. Brazas and D. Ganem, data not shown.
16. J. Polo *et al.*, *J. Virol.* **69**, 4880 (1995).
17. D. W. Lazinski and J. M. Taylor, *ibid.* **67**, 2672 (1993).
18. P.-J. Chen *et al.*, *ibid.* **66**, 2853 (1992); Y. Xia and M. Lai, *ibid.*, p. 6641.
19. C. Lee, J. Lin, M. Chao, K. McKnight, M. Lai, *ibid.* **67**, 2221 (1993).
20. Preliminary alignments with the use of the BLAST algorithm [S. F. Altschul, W. Gish, W. Miller, E. W. Myers, D. J. Lipman, *J. Mol. Biol.* **215**, 403 (1990)] identified three small regions of homology between DIPA and members of the FRA (FOS-related antigen) transcription factor family [D. R. Cohen and T. Curran, *Mol. Cell. Biol.* **8**, 2063 (1988)]. The homology is limited to the bZIP DNA binding and dimerization domain of the FRA proteins and includes both predicted coiled-coil regions of DIPA. The sequence identity between DIPA and rat FRA1 is 35% over the FRA1 bZIP domain.
21. In all figures, pCMV is the new name given to pCEP4 (Invitrogen). The entire HDAg open reading frame was cloned into pCEP4, thereby creating pCMV-HDAg, in which expression of HDAg is under the control of the cytomegalovirus promoter. The pCMV-HDAg ccΔ and ARMΔ expression vectors were constructed by subcloning the mutant HDAg open reading frames from pDL448 and pDL501 (*16*) into pCEP4. The HA epitope tag sequence was cloned as a double-stranded oligonucleotide into the Nco I site present in the *DIPA* cDNA at the native ATG start codon, and the HA-*DIPA* fusion cDNA was then cloned into pCEP4, thereby creating the expression vector pCMV-HA–DIPA. The coiled-coil mutant m1 and m2 *DIPA* open reading frames were created by the insertion of a Bgl II site between codons 67 and 68 and an Sph I site between codons 127 and 128, respectively, with the use of site-directed mutagenesis (Altered Sites II; Promega). 293T cells were transfected by calcium phosphate precipitation [C. Chen and H. Okayama, *Mol. Cell. Biol.* **7**, 2745 (1987)] with the combinations of plasmids (5 μg of each plasmid) shown in Fig. 3. Two days after transfection, the cells were plated in 10-cm plates containing medium supplemented with hygromycin (200 μg/ml) (Boehringer Mannheim). At ~80 to 90% confluence, cells from each plate were harvested and lysed in a solution containing 50 mM tris-HCl (pH 7.5), 400 mM NaCl, 0.2% NP-40, and protease inhibitors. The lysate was adjusted to 100 mM NaCl with buffer lacking NaCl and centrifuged at 100,000*g* for 60 min. The resulting supernatant was subjected to immunoprecipitation as described [E. Harlow and D. Lane, *Antibodies: A Laboratory Manual* (Cold Spring Harbor Laboratory Press, Cold Spring Har-

bor, NY, 1988)] with monoclonal antibodies (12CA5) to HA. Both lysate supernatants and immunoprecipitates were fractionated by SDS–polyacrylamide gel electrophoresis on 12.5 or 15% (for HDAg deletion derivatives) gels, and the resolved proteins were transferred to Immobilon-P (Millipore) membranes and subjected to immunoblot analysis with either polyclonal antibodies to DIPA (1:4000 dilution) (CalTag) or polyclonal antibodies to HDAg (1:15,000 dilution) (CalTag). Immune complexes were detected with horseradish peroxidase–conjugated goat antibodies to rabbit immunoglobulin G (1:7500 dilution) (Gibco BRL) and enhanced chemiluminescence (ECL; Amersham).
22. A. D. Branch *et al.*, *Science* **243**, 649 (1989).
23. D. M. Engelman, T. A. Steitz, A. Goldman, *Annu. Rev. Biophys. Biophys. Chem.* **15**, 321 (1986).
24. A. Lupas, *Methods Enzymol.* **266**, 513 (1996).
25. Supported by Howard Hughes Medical Institute.

29 March 1996; accepted 26 July 1996

Phenotypic Analysis of Antigen-Specific T Lymphocytes

John D. Altman, Paul A. H. Moss, Philip J. R. Goulder, Dan H. Barouch, Michael G. McHeyzer-Williams,* John I. Bell, Andrew J. McMichael, Mark M. Davis†

Identification and characterization of antigen-specific T lymphocytes during the course of an immune response is tedious and indirect. To address this problem, the peptide–major histocompatability complex (MHC) ligand for a given population of T cells was multimerized to make soluble peptide-MHC tetramers. Tetramers of human lymphocyte antigen A2 that were complexed with two different human immunodeficiency virus (HIV)–derived peptides or with a peptide derived from influenza A matrix protein bound to peptide-specific cytotoxic T cells in vitro and to T cells from the blood of HIV-infected individuals. In general, tetramer binding correlated well with cytotoxicity assays. This approach should be useful in the analysis of T cells specific for infectious agents, tumors, and autoantigens.

Quantitative analyses of antigen-specific T cell populations have provided important information on the natural course of immune responses (*1*–*3*). Currently, the standard method for deriving frequency information is limiting dilution analysis (LDA) (*3*). However, this technique may significantly underestimate the number of specific T cells because it cannot detect cells that have no proliferative potential (*4*–*6*). Although flow cytometry provides a fast and direct method for enumerating cells expressing a particular antigen on their surface, detection of low-frequency populations of antigen-specific lymphocytes by staining with their cognate antigen has only been demonstrated for B lymphocytes, making use of the high affinity for antigen that many of these cells have (*7*). Antigen-specific T cells from normal, immunized mice have been identified and analyzed in a few systems, with T cell receptor V region antibodies as surrogate markers for antigen specificity (*1*, *8*), but the more general approach of staining specific T cells with their ligand has failed because soluble peptide-MHC complexes have an inherently fast dissociation rate from the T cell antigen receptor (*9*).

Multimeric peptide-MHC complexes should be able to bind more than one T cell receptor (TCR) on a specific T cell, and thus have correspondingly slower dissociation rates, making the complexes more suitable for use as an immunological stain. To engineer tetrameric peptide–MHC complexes, we first added a 15–amino acid substrate peptide for BirA-dependent biotinylation (*10*) to the COOH-terminus of the human lymphocyte antigen (HLA)–A2 heavy chain. After folding the heavy-chain fusion protein in vitro in the presence of β_2-microglobulin (β_2M) and a specific peptide ligand (*11*), the purified MHC-peptide complex was biotinylated efficiently (70 to 100%) on a single lysine within the BirA substrate peptide (BSP) (*12*). Biotinylation at the COOH-terminus of the heavy chain also served to correctly orient the MHC molecule, as the site recognized by the TCR involves the NH_2-terminal domains (*13*). Tetramers were produced by mixing the biotinylated peptide–MHC complex with phycoerythrin-labeled deglycosylated avi-

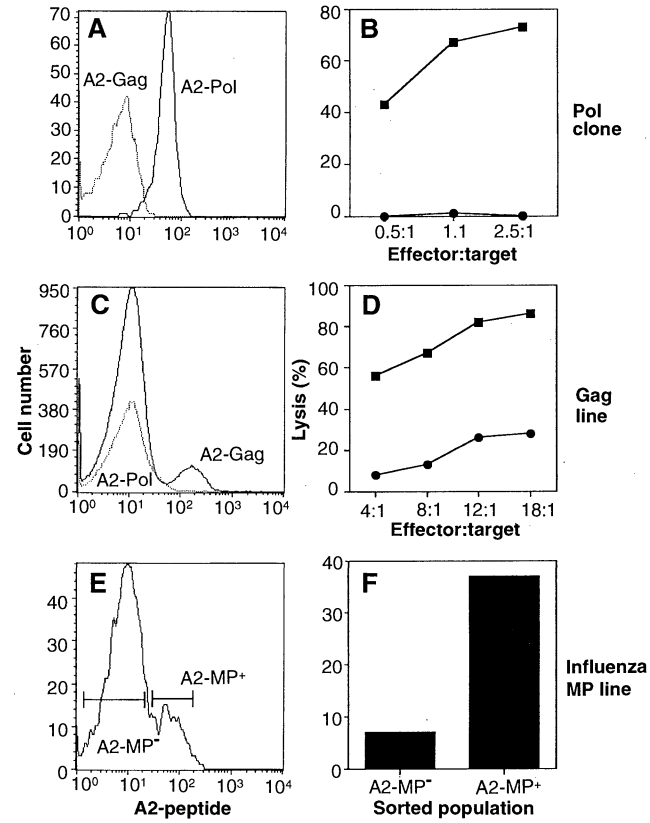

Fig. 1. Staining by MHC-peptide tetramers correlates with peptide-dependent cytotoxicity. Flow cytometric analysis (*18*) of $CD8^+$ T cells (*17*, *20*, *30*) from (**A**) clone 20 stained with A2-Pol (solid line) and A2-Gag (dotted line) tetramers, (**C**) HIV-Gag–specific CTL line 868 stained with A2-Gag (solid line) and A2-Pol (dotted line) tetramers, and (**E**) an HLA-A2–restricted influenza matrix peptide CTL line (PG-001), stained with A2-MP tetramers and sorted into A2-MP^+ and A2-MP^- populations, as indicated. Cytotoxicity assays with (**B**) clone 20 showed specific killing of autologous Epstein-Barr virus–transformed B cells pulsed with Pol peptide (closed squares) but not target cells without added peptide (closed circles). (**D**) The 868 Gag–specific CTL line killed cells pulsed with the Gag peptide (closed squares) but not target cells without added peptide (closed circles). (**F**) The sorted populations from (E) were assayed for killing of MP-pulsed target cells at an effector:target ratio of 1:1. At the same ratio, in cells not treated with peptide, no killing of target cells was seen.

J. D. Altman and M. G. McHeyzer-Williams, Department of Microbiology and Immunology, Stanford University School of Medicine, Stanford, CA 94305–5428, USA.
P. A. H. Moss, P. J. R. Goulder, D. H. Barouch, J. I. Bell, A. J. McMichael, Institute for Molecular Medicine, John Radcliffe Hospital, Headington, Oxford OX3 9DU, UK.
M. M. Davis, The Howard Hughes Medical Institute, Department of Microbiology and Immunology, Beckman Center, Room B221, Stanford University, Stanford, CA 94305–5428, USA.

*Present address: Department of Immunology, Duke University Medical Center, Durham, NC 27707, USA.
†To whom correspondence should be addressed.